Comparison of Auger Coefficients in Type I and Type II Quantum Well Midwave Infrared Lasers

Jerry R. Meyer, *Fellow, IEEE*, Chadwick L. Canedy, Mijin Kim, Chul Soo Kim, Charles D. Merritt, William W. Bewley, and Igor Vurgaftman

***Abstract*— We perform a detailed comparison of 2D Auger coefficients in narrow-gap type-I and type-II quantum wells (T1QWs and T2QWs), and the relative effects of Auger non-radiative decay on midwave infrared lasers employing both types of gain media. Comparison is also made to 3D Auger coefficients in bulk mid-IR materials, by defining a "normalization length" that accounts for the spatial extent of the electron and hole wavefunctions in the quantum wells. The comparisons confirm that Auger recombination in both types of QW is substantially suppressed relative to bulk, due primarily to the effects of compressive strain on the valence subband dispersions. We find that the 2D Auger coefficients in T1QWs remain substantially lower than those in T2QWs out to wavelengths beyond 3.5 μm. However, this does not necessarily imply a lower lasing threshold because a substantial fraction of the holes injected into T1QWs occupy lower subbands that do not contribute gain, so more must be injected to reach the lasing threshold. When all of the relevant considerations are combined, the thresholds for the best T1QW and T2QW lasers cross over near $\lambda \approx 3.0$ μm. Other characteristics governing the relative T1QW and T2QW laser performances above threshold, such as maximum output power and wallplug efficiency, are also considered.**

***Index Terms*— Auger recombination, diode laser, laser threshold, midwave infrared.**

I. Introduction

ONGOING advances in semiconductor laser and detector technologies for the midwave infrared (mid-IR, loosely defined here as 2-6 μm) have substantially expanded their use in systems addressing such commercial and military applications as chemical sensing [1]–[3], infrared countermeasures [4], and thermal imaging [5], [6]. For interband lasers operating in the mid-IR, threshold current densities are nearly always limited by the non-radiative Auger process, in which electron-hole recombination is accompanied by the excitation of a third carrier (either electron or hole) to an excited state that conserves energy and momentum [7], [8]. Whereas the carriers injected electrically to produce population inversion and gain can also recombine by radiative or Shockley-Read (defect-assisted) processes, the multi-carrier Auger mechanism tends to dominate at high carrier concentrations, so long as the operating temperature is high enough to overcome the activation energy associated with the energy gap. Auger recombination can also affect the laser damping factor, optical feedback dynamics [9], and dark current in mid-IR photodetectors, although it is less likely to dominate in detectors since they typically operate at very low optical excitation levels, and often at cryogenic temperatures to maximize the detection sensitivity.

Previous studies have analyzed and characterized the effects of Auger recombination on specific types of mid-IR lasers and detectors [10]–[19]. However, no previous work has comprehensively compared that role across classes, or fully deconstructed the physical basis for the wavelength range over which each class of devices is advantageous. In particular, type-I quantum well (T1QW) lasers (with electron and hole wavefunctions concentrated in the same layer) are generally acknowledged to perform optimally at $\lambda < 2.8$ μm, whereas type-II QW (T2QW) devices (with electron and hole wavefunctions concentrated in adjacent layers) are preferable at $\lambda > 3.5$ μm. However, little guidance has been available concerning how their differing Auger coefficients and carrier distributions among the QW subbands affect the competition for dominance in the intermediate range ($\approx$ 2.8-3.5 μm). We will show in the following Sections that the Auger coefficient alone does not reliably predict which QW configuration minimizes the threshold current density, or overall laser performance.

II. Auger Recombination and Its Experimental Characterization

In an Auger process, the energy of a recombining electron-hole pair (which must exceed the bandgap, Eg) is transferred to a third carrier that jumps to an excited state in either the conduction or valence band.7 Since three carriers are required for this to occur, the decay rate scales (nominally, for nondegenerate statistics) as $n^2 p$ or np^2, depending on whether the third carrier is an electron or hole. Here n and p are the 3D (or 2D sheet) electron and hole densities that populate the bulk (or QW) material.

Because the third carrier's final state must conserve the net energy and momentum of all three initial carriers, the Auger decay rate is quite sensitive to details of the bulk or QW band structure [8]. For the example of an *nnp* process in

Manuscript received April 6, 2021; revised June 15, 2021 and June 29, 2021; accepted July 5, 2021. Date of publication July 12, 2021; date of current version July 27, 2021. *(Corresponding author: Jerry R. Meyer.)*

Jerry R. Meyer, Chadwick L. Canedy, Chul Soo Kim,Charles D. Merritt, William W. Bewley, and Igor Vurgaftman are with the U.S. Naval Research Laboratory, Washington, DC 20375 USA (e-mail: jerry.meyer@nrl.navy.mil).

Mijin Kim is with Jacobs, Hanover, MD 21076 USA.

Color versions of one or more figures in this article are available at https://doi.org/10.1109/JQE.2021.3096219.

Digital Object Identifier 10.1109/JQE.2021.3096219

a bulk semiconductor with wide direct bandgap (emitting in the near IR or visible), such as GaAs or $In_xGa_{1-x}As$, it becomes difficult to conserve both energy and momentum because at least one of the three initial carriers must have a momentum nearly as large as that of the final electron which occupies a state at least a full bandgap above the conduction band minimum. Hence the process has a large activation energy proportional to E_g. The energy required to activate a *ppn* process is even more prohibitive, unless an intervalence resonance comes into play as will be discussed below.

On the other hand, the band structure of a narrow-gap bulk material such as InAs, InSb, or $Hg_{1-x}Cd_xTe$ is quite conducive to rapid nnp Auger decay. Since the heavy hole has a large effective mass (typically $\approx$ 0.35-0.4 m_0) whereas the much smaller electron mass scales with energy gap, the initial hole can have a large wavevector without much energy (and therefore a relatively high occupation probability), whereas the final electron can have a large energy ($\approx E_g$) without much momentum. It follows that the activation energy for this process is quite small. Multi-hole Auger processes can also conserve energy and momentum if the energy gap is roughly equal to the separation of the valence band maximum and a lower valence band or subband at $k = 0$. For example, the split-off gap nearly equals the energy gap in bulk InAs or $InAs_{1-x}Sb_x$ [20]. Based on these fundamental considerations that unavoidably cause Auger non-radiative decay rates to be high in bulk narrow-gap semiconductors, it was long considered unlikely that diode lasers emitting in the mid-IR would ever attain thresholds low enough to allow room temperature operation.

In the mid-1990s, however, Grein, Flatté and co-workers pointed out that with band-structure engineering, type-II InAs-Ga(In)Sb quantum wells and superlattices (SLs) lattice-matched to GaSb can have Auger rates much lower than in bulk materials such as $Hg_{1-x}Cd_xTe$ with the same energy gaps [11], [13]. Furthermore, this assertion was confirmed by experimental observations [12]. In these quantum heterostructures, compressive strain splits the degeneracy between heavy and light holes at $k = 0$, and the in-plane effective mass for the uppermost heavy hole subband becomes light (similar to that of the electrons) near the zone center. This is illustrated in Fig. 1, which plots the in-plane dispersion relations for the two lowest electron and two highest hole subbands in an InAs/GaInSb/InAs AlSb type-II "W" quantum well [21] with conduction and valence band profiles shown in the inset. Since the electron and hole effective masses are roughly equal near the zone center, any hole state with wavevector large enough to conserve momentum in an nnp Auger process has much larger energy than in bulk, and is consequently far less likely to be occupied at room temperature. Hence a significant activation energy is induced. A number of subsequent experiments at NRL [22], [23] and elsewhere [24] confirmed the strong suppression of Auger recombination in mid-IR type-II InAs-Ga(In)Sb-based QWs and SLs compared to bulk materials with the same energy gaps, as will be seen below.

It was also suggested that *ppn* Auger decay rates may become quite sensitive to valence subband alignments that could induce resonant Auger processes [11]. Subsequent

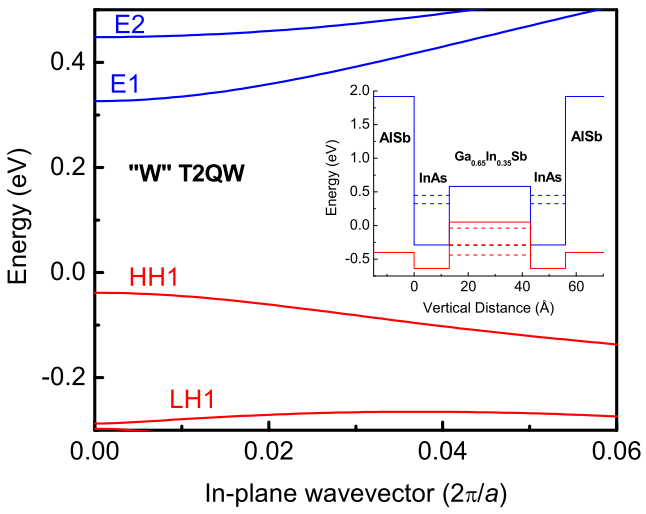

Fig. 1. In-plane dispersion relations for the two lowest electron and two highest hole subbands in an InAs/$Ga_{0.65}In_{0.35}Sb$/InAs/AlSb (13Å/30Å/13Å/30Å) type-II "W" quantum well. The inset illustrates the conduction and valence band profiles for the four constituents, along with energy levels of the lowest electron and highest hole subbands (dashed lines).

experiments established that *ppn* Auger rates in T2QWs can indeed be substantial, although they failed to establish any systematic correlation with specific valence intersubband alignments relative to the energy gap. This is probably due to the wide diversity of transitions that can occur, in conjunction with broadening of the inter-level spacings by non-uniformities in the quantum well thickness [22]. An experiment that varied the hole/electron density ratio at the threshold of a mid-IR laser with type-II "W" active QWs found roughly equal Auger coefficients for *nnp* and *ppn* processes [25]. Because the electron and hole masses in optimized T1 and T2 QWs are roughly equal, and numerous valence intersubband transitions are usually possible, both *nnp* and *ppn* processes most likely contribute to the Auger recombination in both T1 or T2 QWs [11]. To date, no reliable experimental evidence indicates which process dominates.

Compared to wider-gap gain materials, strained narrow-gap T2QWs have the advantage of a smaller band-edge density of states, which reduces the carrier density required to reach population inversion. Defying earlier expectations, this and the strong Auger suppression associated with the T2QW band structure allowed mid-IR T2QW lasers, in particular the interband cascade laser (ICL) [26], [27], to display low thresholds and high output powers (up to 500 mW) when operated in continuous wave (cw) mode at room temperature.[17]

Following the prediction and experimental confirmation of substantial Auger suppression in T2QWs compared to bulk materials, it was generally taken for granted that they also have smaller Auger coefficients than mid-IR T1QWs with the same bandgaps. This supposition was supported by the measurement of a relatively high Auger coefficient for a type-I $InAs_{0.85}Sb_{0.15}$-$In_{0.87}Al_{0.13}As_{0.91}Sb_{0.09}$ multiple quantum well (MQW) [28]. However, several groups subsequently showed that mid-IR InGa(As)Sb T1QWs, with GaSb or AlGa(In)AsSb barriers and grown on GaSb with much greater strain, can also

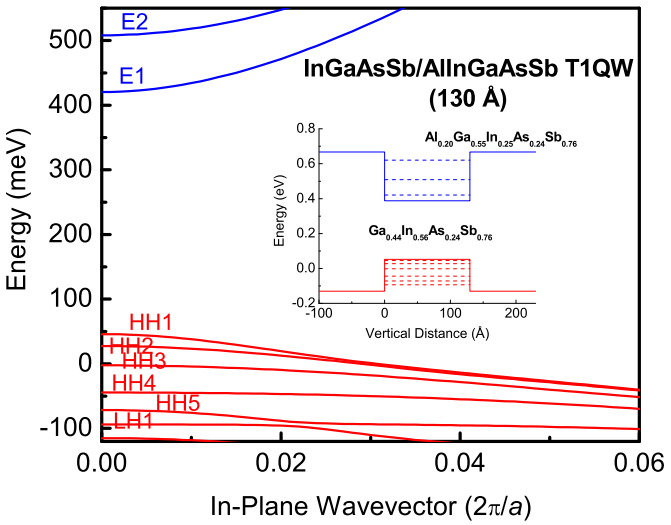

Fig. 2. In-plane dispersion relations for electron and hole subbands in a 130-Å-thick $Ga_{0.44}In_{0.56}As_{0.24}Sb_{0.76}/Al_{0.20}Ga_{0.55}In_{0.24}As_{0.24}Sb_{0.76}$ T1QW that is similar to one of those described in [29]. The inset shows the conduction and valence band profiles, along with energy levels for the electron and hole subbands (dashed lines).

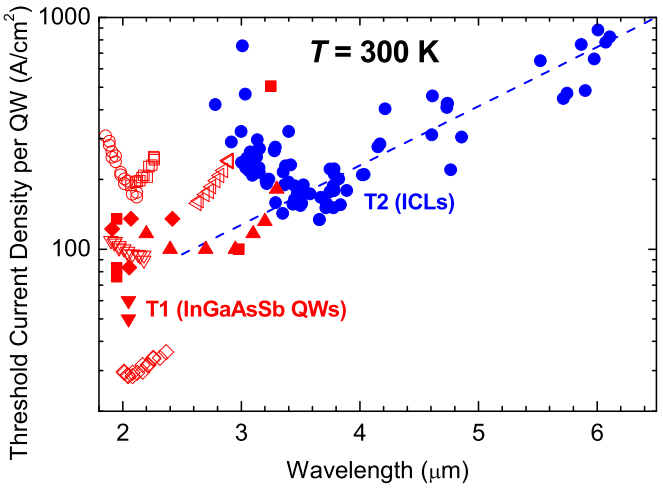

Fig. 3. Threshold current density per quantum well per active stage *vs.* wavelength for T1 InGaAsSb QW and T2 interband cascade lasers[17] operating at room temperature. The T1 lasers were reported by U. Surrey [16], [19], [34] (all open red points), MIT Lincoln Lab [28] (filled upside-down triangles), SUNY diodes [29], [35]–[39] (filled triangles), SUNY T1 ICLs (filled squares) [30], and Brolis [40] (filled diamonds). The blue dashed curve is a guide to the eye.

display significant suppression of the Auger decay rate [13], [16], [17], [19]. This is not really surprising since, as in T2QWs, compressive strain splits the valence band degeneracy at $k = 0$ and induces a much lighter in-plane heavy hole mass near the zone center. Figure 2 illustrates the dispersion relations of various electron hole subbands in a typical InGaAsSb/AlInGaAsSb QW that may be used to produce gain in a mid-IR T1QW laser (with bandgap corresponding to $\lambda = 3.3$ μm in this example). Again, the inset shows band profiles and subband energies. Whereas quaternary AlGaAsSb barriers are sometimes employed, the quinternary barrier shown here provides a larger valence band offset. GaSb barriers are unfavorable for lasers because they provide almost no valence band offset to confine the holes.

University of Surrey and NRL recently reported a detailed quantitative investigation of Auger coefficients in mid-IR T1QWs [19]. Besides confirming the substantial suppression of *nnp* Auger recombination, that work also quantified the Auger coefficient's systematic *increase* at wavelengths for which the energy gap comes into resonance with the split-off gap [16]. Again due to strong Auger suppression, T1QW lasers emitting in the 2-3.4 μm spectral range, including ICLs with type-I active transitions [30], have reached high performance levels, with thresholds among the lowest reported for any edge emitting semiconductor laser, regardless of wavelength [31].

Figure 3 plots the threshold current densities per quantum well per active stage for single-stage GaSb-based T1 (red) and multi-stage T2 (blue) QW lasers operating at a broad range of mid-IR wavelengths, where the blue dashed curve is a guide to the eye. The T2QW devices are seen to have lower thresholds per QW at wavelengths down to at least $\approx$ 3.4 μm. A caveat is that whereas all of the T2QW thresholds were obtained for broad-area devices with 2-mm-long cavities, the T1QW data represent a range of cavity lengths, and some were narrow ridges that are subject to higher scattering loss. It should also be mentioned that since most of the T1QW lasers have 2-3 wells per stage and the type-II ICLs have 3-10 stages that must be biased in series, the relative threshold input power density ($j_{th} \times V_{\rm th}$) may look quite different from the comparison in this figure, as will be discussed further below.

III. Determination of Auger Coefficients From Lasing Thresholds

Since Auger recombination strongly dominates the threshold current densities in both T1 and T2 interband mid-IR lasers operating at room temperature, we can extract Auger coefficients from the $J_{\rm th}$ data, provided the internal losses, internal efficiencies, and optical confinement factors are sufficiently well known. We also need a reliable model for the modal optical gain, which can be used to extract the electron and hole densities required to reach threshold. NRL has used this approach to extract Auger coefficients in T2 ICLs emitting at a broad range of wavelengths [15], [18], [23], and most recently in mid-IR T1QW laser structures [19]. However, no systematic comparison of the T1 and T2 QW results has been reported previously.

Because the optically- or electrically-injected carrier concentrations needed to produce gain nearly always exceed the doping concentration, we assume $p \approx n$ (although this may not strictly apply to ICLs [25]). The Auger recombination rate for non-degenerate statistics is then proportional to n^3, although as the carriers become degenerate at higher concentrations the rate begins to saturate and increase somewhat less rapidly than n^3 [24]. The lifetime corresponding to the cubic dependence is $\tau_{\rm A} \approx 1/C_{\rm 2D}n^2$, where $C_{\rm 2D}$ is the 2D Auger coefficient with units $\rm cm^4/s$. The same expression may be applied to bulk materials if we substitute the bulk carrier concentration and 3D Auger coefficient $C_{\rm 3D}$ with units $\rm cm^6/s$.

The total threshold current density for lasing is the sum of the radiative and non-radiative contributions, with Auger recombination strongly dominating the latter in state-of-the-art mid-IR QW gain media, as mentioned above.

The non-radiative component is then :

$$J_{\text{Auger}}^{\text{3D}} = eLC_{\text{3D}}n_{th}^3 \tag{1a}$$

in bulk or :

$$J_{\text{Auger}}^{\text{2D}} = eN_{\text{QW}}C_{\text{2Dv}}n_{\text{th}}^3 \tag{1b}$$

in a QW. Here, e is the electronic charge, L is thickness of the bulk gain region, n_{th} is the 3D or 2D threshold carrier density (per QW in 2D), and N_{QW} is the number of active wells (which we assume to be populated equally). Note that we set $N_{\text{QW}} = 1$ for an ICL because the same threshold current populates the single active QW in each stage.

The contribution of radiative recombination to the threshold current density may be determined experimentally by measuring the temperature dependence of the spontaneous emission at threshold, or it may be estimated theoretically. It was found that at room temperature the radiative component for T1 devices accounts for approximately 20% of J_{th} [19], whereas for T2 devices the fraction is much smaller. Therefore, if we can reliably calculate the threshold carrier density n_{th} for a given laser in conjunction with measurement of its threshold current density, we can use Eq. (1a) or (1b) to extract the Auger coefficient C_{3D} or C_{2D} for the active gain material of that device. To calculate n_{th} for each laser, we simulated the optical gain using an 8-band $\mathbf{k}\cdot\mathbf{p}$ theory with the reciprocal space method [8]. The gain required to induce lasing was determined using experimental values for the cavity and mirror losses, where available, along with the optical confinement factor corresponding to the specified layering of the waveguide structure. We neglect Joule heating of the QWs, which is generally modest at the lasing threshold. We also neglect effects of the electric field applied to inject current, since they are most likely smaller than experimental uncertainties in the Auger coefficient.

As an example of this procedure, we consider a broad-area T1QW laser with three active wells, cavity length 0.5 mm, and uncoated facets emitting at $\lambda = 2.37$ μm [19]. The internal loss for this laser was determined experimentally to be 4 cm^{-1}, which implies a total threshold gain of 26.5 cm^{-1}. The procedure outlined above (including a model of the optical waveguide to determine the confinement factor) calculates that $n_{\text{th}} = 1.06 \times 10^{12}$ cm^{-2} is required to reach this gain. The corresponding radiative current per QW is then 9.5 A/cm^2. This particular laser displayed a low measured threshold current density of 108 A/cm^2 (36 A/cm^2 per QW), from which the Auger component is 26.5 A/cm^2 per QW and $C_{\text{2D}} = 1.4 \times 10^{-16}$ cm^4/s. The corresponding Auger lifetime is 6.4 ns, and the total lifetime including both radiative and nonradiative contributions is 4.7 ns. Threshold carrier densities for most of the other T1QW lasers discussed below are in the 1.0-1.5 $\times$ 10^{12}cm^{-2} range, while the carrier lifetimes vary from $\approx$ 1 to 4 ns, with the lower values typically observed at longer wavelengths.

For T2QW ICLs with the band structure illustrated in Fig. 1 [20], only one electron (hole) subband is typically occupied. Even though the electron and hole densities are not necessarily the same, they can be nearly equalized by adjusting the doping level in the electron injector (carrier rebalancing) [25]. This leads to a relatively low threshold carrier density of $n_{\text{th}} = 6.5 \times 10^{11}$ cm^{-2} for a typical 2-mm-long uncoated broad-area laser with internal loss 5 cm^{-1} ($g_{\text{th}} \approx 10.5$ cm^{-1}). The radiative current density at threshold is then computed to be $\approx$ 3 A/cm^2, a small fraction of the total measured threshold current density of 150-200 A/cm^2. The radiative current is much lower than in the T1QW example because the optical matrix element and threshold carrier density are both reduced. Assuming an internal quantum efficiency of 80%, we obtain $C_{\text{2D}} \approx 3 \times 10^{-15}$ cm^4/s and a carrier lifetime of 0.6-0.8 ps.

Although this procedure extracts a 2D Auger coefficient from the QW laser threshold, and all state-of-the-art III-V mid-IR lasers employ T1 or T2 QWs instead of bulk materials, it is nonetheless convenient to relate the 2D values to a 3D representation so comparison may also be made to bulk mid-IR materials [22]. Moreover, most previous investigations of Auger recombination in QWs have reported 3D rather than 2D Auger coefficients (*e.g.*, [17], [41]–[43]), so a conversion is needed, at the very least, to place the earlier studies in context. We accomplish this transformation by calculating a normalization length corresponding to the quantum-confined carrier's spatial extent along the growth axis, which may be derived using the wavefunctions ψ_{e} and ψ_{hh} for the relevant electron and hole subbands [15]. The resulting relationship of 3D and 2D Auger coefficients is then:

$$C_{\text{3D}} \approx C_{\text{2D}} \frac{\int |\psi_{\text{e}}|^2 \, \text{dz}}{|\psi_{\text{e}}|^2_{\text{max}}} \frac{\int |\psi_{\text{hh}}|^2 \, \text{dz}}{|\psi_{\text{hh}}|^2_{\text{max}}} \tag{2}$$

The normalization length for a T1QW is typically a fraction of the QW width W (with $C_{\text{3D}} = C_{\text{2D}}W^2/4$ in the limit of infinite barriers), whereas for a T2 InAs-GaInSb-InAs-AlSb "W" QW such as those used in ICLs it tends to be roughly equal to the GaInSb hole QW thickness. Other definitions of normalization length are certainly possible and can be encountered in the literature, so care must be exercised in any detailed quantitative comparison across different published works. Nevertheless, the main trends remain the same regardless of the precise definition of normalization length, and the fast variation with wavelength reduces the importance of numerical factors of order 1. Note that Auger coefficients in photodetectors based on type-II superlattices must also be carefully normalized to be comparable to values in bulk absorbers because the electron-hole overlap is generally well below unity. Overall, we believe the definition in Eq. (2) can be applied meaningfully to a wide variety of band structures and Auger mechanisms.

IV. "3D" Auger Coefficients

In earlier works, Eq. (1b) was used to extract 2D Auger coefficients from the experimental threshold current densities of ICLs emitting at wavelengths between 2.8 and 6.2 μm [15],

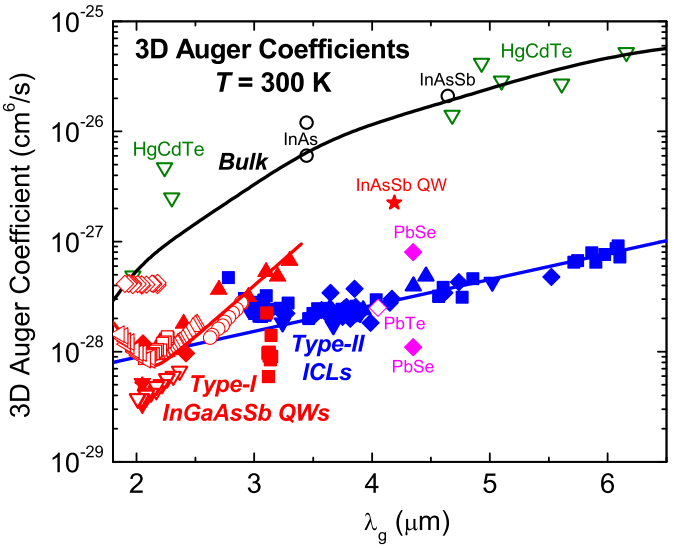

Fig. 4. Auger coefficients *vs*. wavelength (corresponding to the energy gap), as extracted from T1 (red) and T2 [18] (blue) QW laser thresholds at room temperature. The T1QW results include laser data (same symbols as in fig. 3) as well as non-laser Auger results reported by U. CO/U. TX/LANL [17] (filled squares), and NRL/MIT-LL [28] (filled star). For this plot, the 2D Auger coefficients derived from laser threshold experiments were converted to 3D as discussed in the text. Also shown are literature values for various bulk III-V (black), II-VI (green), and IV-VI (magenta) binary and alloy semiconductors. The three curves are guides to the eye.

[18], [32]. Equation (2) was then used to compare the converted 3D values to Auger coefficients in bulk binary and alloy semiconductors with energy gaps spanning the same range.

Figure 4 expands that analysis by including the converted 3D results for T1QWs (red points) [16], [17], [19], [29], [30], [33]–[40]. The open red points are extracted from threshold data acquired at University of Surrey using hydrostatic pressure to vary the bandgap, and hence the emission wavelength, of a given device [19]. This allowed single lasers to span wavelength ranges up to 350 nm. The results are compared to the most complete data set for ICLs with T2 "W" active QWs (blue points) [18], which were extracted from the pulsed thresholds for broad area lasers with standard dimensions at 300 K. Also shown in Fig. 4 are the Auger coefficients reported for various bulk III-V (black) [28], [44], II-VI (green) [45]–[49], and IV-VI (magenta) [50], [51] semiconductors with energy gaps in the same mid-IR range.

The C_{3D} values derived from type-II ICL thresholds are remarkably consistent, with fluctuations at a given wavelength rarely exceeding a factor of 2. This is despite the extraction from data acquired over an 11 year period, from lasers processed from 70 different wafers with stage multiplicities ranging from 3 to 10 and employing a wide variety of active QW and waveguide designs. The T1QW results for structures grown at a number of different facilities are also largely consistent. One exception is a hydrostatically-tuned InGaAsSb/AlGaAsSb MQW laser, whose values are an order of magnitude higher at wavelengths between 1.9 and 2.2 μm (open red diamonds). That structure displayed no obvious deficiencies in layer design or growth/processing quality [19], although its QWs were thinner (80 Å) than for any of the other T1QWs (100-130 Å).

The other anomaly is the much lower T1QW Auger coefficients reported recently for InGaAsSb/GaSb MQWs with bandgaps near 3.1 μm (red squares) [17]. That study extrapolated C_{3D} values to the limit of non-degenerate carrier populations as a function of compressive strain on the QWs, which was induced both epitaxially and mechanically. The low C_{3D} values are probably associated with the use of GaSb rather than AlGa(In)AsSb barriers to bound the InGaAsSb QWs. Note that whereas Eq. (2) accounts for the spatial distribution of carrier wavefunctions localized in the QW, the valence band offset for structures with GaSb barriers was only 0-75 meV [17]. Consequently, many of the optically-injected holes would not have been confined to the QWs at all, instead occupying the extensive surrounding GaSb layers. Thus the Auger coefficients may have been artificially suppressed by weak wavefunction overlap of the unbound holes with electrons localized in the QWs. As mentioned above, the very low valence band offset and weak hole confinement provided by GaSb barriers makes them disadvantageous in T1QW lasers.

Deferring examination of the wavelength dependences for T1 and T2 QW Auger coefficients to the next Section, we emphasize here the dramatic contrast with bulk materials. Figure 4 confirms that the lighter hole mass near the valence band maxima of a compressively-strained QW indeed induces a strong suppression of the Auger non-radiative decay, enabling mid-IR lasers incorporating QWs of both types to display low thresholds. In contrast, the Auger coefficients for bulk III-V and II-VI (HgCdTe) materials increase with wavelength by two orders of magnitude between 2 μm and 6 μm. The exceptions are PbSe and PbTe (magenta points), which also have very low Auger coefficients. One result reported for PbSe [50] is lower for its wavelength of 4.4 μm than any of the QW values. This is due to the very different band structure of narrow-gap lead chalcogenides, which features mirror-image electron and hole dispersions at the four degenerate L-points, rather than the light electron and heavy hole masses characteristic of InAs or HgCdTe.

V. 2D Auger Coefficients

Whereas the conversion to 3D provides a meaningful comparison of T1 and T2 QW Auger coefficients to bulk values, the 2D coefficients extracted directly from the threshold analysis are naturally more relevant to QW laser operation. Figure 5 replots the T1 and T2 Auger coefficients from Fig. 4 in the 2D representation, excluding T1QW structures with GaSb barriers that are less favorable for lasing. For both QW types, the main trends as a function of wavelength are naturally quite similar in the 2D and 3D representations.

At longer wavelengths, the coefficients increase exponentially because Auger recombination is an activated process. Note, however, that after passing through minima the trends for both QW types increase again with decreasing wavelength. It is well documented that this occurs in T1 InGaAsSb QWs because at wavelengths somewhat shorter than 2 μm, the bandgap moves into resonance with the split-off gap [16],

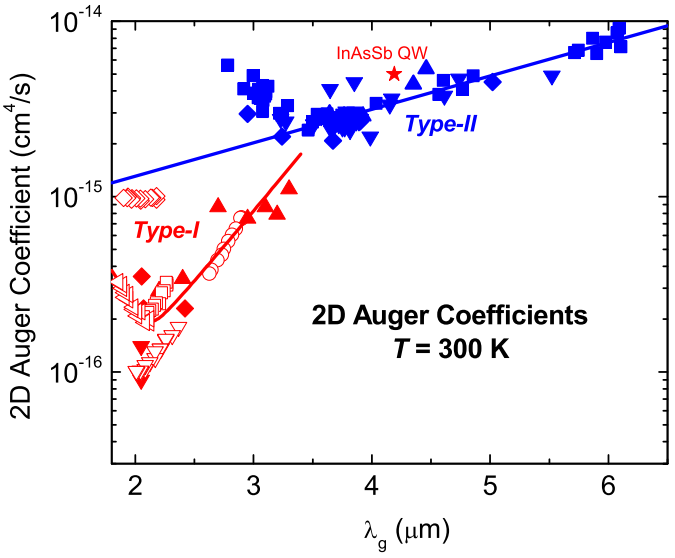

Fig. 5. 2D Auger coefficients *vs*. wavelength extracted from laser thresholds at room temperature, based on the T1 [16], [19], [29], [30], [35]–[40] (red) and T2 [18] (blue) QW data used to generate fig. 4 (same symbols) but excluding T1QW structures with GaSb barriers. The red and blue curves are again guides to the eye.

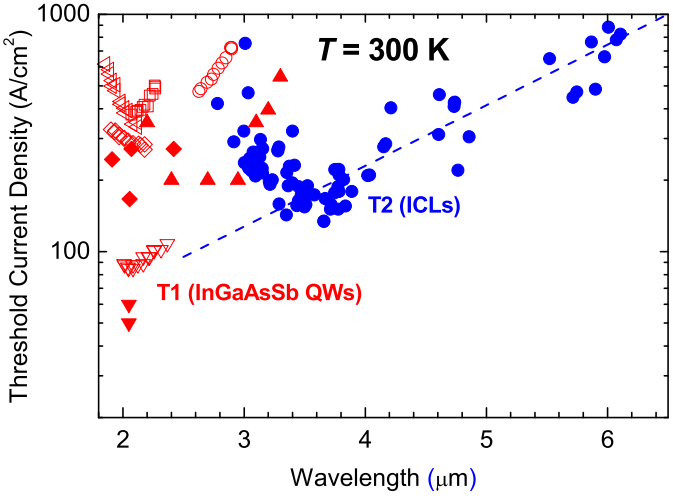

Fig. 6. Total threshold current density *vs*. wavelength for the same T1 and T2 QW lasers whose thresholds per QW per stage are plotted in fig. 3. The blue curve is again a guide to the eye.

[20]. In that regime it is straightforward to conserve both energy and momentum via *ppn* Auger processes in which the electron recombination with a heavy hole excites a second heavy hole to the spin-orbit split off valence subband. This process also limits InP-based QW lasers operating in the 1.3-1.6 μm range [52].

The reason for the increase of C_{2D} in T2QWs at wavelengths shorter than $\approx$ 3.2 μm is unknown at present, but occurs regardless of where the ICLs are designed, grown and processed [53]. Similar minima in j_{th} at $\lambda \approx 3.2$ μm and $\approx$ 3.5 μm were observed at U. Surrey when hydrostatic pressure was applied to vary the bandgap of two ICLs [54], [55]. Furthermore, the unexpected behavior of the Auger coefficient is accompanied by an increase of the internal loss in the same shorter-wavelength range [18]. Theoretical simulations based on current models for the ICL band structure, carrier dynamics, and mode properties predict that both the Auger coefficient and internal loss should continue to decrease down to wavelengths much shorter than 2.5 μm. For comparison, the Auger coefficients for near IR InGaAs QW lasers grown on InP are typically in the 10^{-29} cm^6/s range in 3D units, which corresponds to the 10^{-17} cm^4/s range in 2D [19], [41], [42]. The coefficients for InGaAs-GaAs lasers emitting at shorter wavelengths are even lower [43].

Whereas considered individually the overall wavelength trends for both QW types look quite similar in the 3D and 2D representations, note that the relative magnitudes of C_{2D} in T1 *vs*. T2 QWs have shifted appreciably. In particular, in 2D the T1QW values appear much more advantageous out to wavelengths as long as $\approx$ 3.5 μm. That shift results from the much wider normalization lengths for T1QWs, which are typically $\approx$ 55, 64, or 79 Å for T1QW thicknesses of 80, 100, or 130 Å, respectively, as compared to $\approx$ 40 Å for the T2 "W" QWs. Thus if the 3D carrier concentrations and lifetimes in T1 and T2 QWs are equal, the T1QW has a much higher 2D concentration and consequently, from $C_{2D} = 1/n^2\tau_A$, a much lower Auger coefficient. So long as all the injected electrons and holes occupy states in the lowest conduction and highest valence subbands that produce gain, a lower C_{2D} correlates directly with lower threshold current density for lasing (assuming similar optical confinement factors and net losses).

However, whereas C_{2D} determines the non-radiative decay rate based on the total sheet carrier concentration per QW, the fraction of those carriers populating "useful" subbands that actually produce gain is quite different in state-of-the-art designs for the two types of QWs. For example, a statistical calculation at room temperature for the T1QW band structure illustrated in Fig. 2 finds that 88% of the electrons reside in the lowest subband and most of the other 12% in the second. On the other hand, the close spacing the valence subbands makes them almost bulk-like. Only 35% of the holes reside in the uppermost HH1 subband, with 28% in the second, 25% in the third, 10% in the fourth, and 2% in fifth. The simulation estimates that whereas the lasing threshold is reached with a hole density of 3.3×10^{11} cm^{-2} in the HH1 subband, 9.3×10^{11} cm^{-2} total holes must be injected to reach that "useful" concentration. For T1QWs with the thinnest QW thicknesses of 80 Å, the electron (hole) populations in the lowest (highest) subbands are only moderately higher, with 95% of the electrons in E1 and 42% of the holes in HH1.

By contrast, both conduction and valence intersubband separations in the T2QW of Fig. 1 are large enough that for injection corresponding to the lasing threshold at room temperature, the fraction of carriers occupying higher subbands is negligible. It follows that simply comparing 2D Auger coefficients for T1 and T2 QWs provides a misleading indicator of which QW type can lase with lower threshold carrier density.

One could consider defining a "handicapped" Auger coefficient that accounts for the distribution of carriers between the

subbands: $C_{2D}^{h} \equiv (n/n_{E1})^2(p/p_{HH1})C_{2D}$ for *nnp* processes or $(n/n_{E1})(p/p_{HH1})^2C_{2D}$ for *ppn* processes. The implicit assumption here that a single Auger coefficient governs carriers occupying all the subbands is reasonable, because intersubband thermalization occurs on a time scale much faster than the recombination lifetime. However, we stop short of implementing this approach because of its fundamental similarity to simply employing the threshold current density itself as the figure of merit. It differs only in separating the lifetime and its dependence on band structure from other factors such as multiplicity of QWs, optical confinement factor, waveguide loss, and optical matrix element (which is higher in a T1QW due to stronger overlap of the electron and hole wavefunctions). And of course it would not be meaningful to apply such handicapping to IR detectors, since their dark currents are nominally insensitive to carrier distribution between the subbands.

Because the total threshold current density is ultimately of greater interest than the threshold per QW, Fig. 6 replots the data from Fig. 3 in that form. We find that the net thresholds for T2QWs remain lower for wavelengths down to at least ≈ 3.1 μm, although this still fails to tell the whole story as will be discussed in the next Section.

VI. Other Considerations

We see from Figure 6 that the thresholds for T1 and T2 QW lasers cross over near $\lambda \approx 3.1$ μm. However, it was mentioned above that the multiple stages in an ICL require higher operating voltage than for a non-cascading InGaAsSb QW diode. Although it is not feasible to plot threshold power densities (P_{th}) corresponding to the j_{th} data shown in Fig. 3, because most of the references did not provide *I-V* curves or otherwise specify the threshold voltage (V_{th}), we can nonetheless use whatever information is available to estimate the differing voltage requirements. A survey of the best data for T1 InGaAsSb QW lasers yields that at $\lambda = 2.03$ μm, a narrow-ridge laser with 3 active QWs from SUNY operated with threshold voltage 0.9V [56]. At the somewhat longer wavelength $\lambda \approx 2.7$ μm, a DFB laser with 6 active QWs from JPL operated with threshold voltage 1.05 V [57], while a broad-area device with 2 QWs from Walter Schottky Institut displayed $V_{th} = 0.75$ V [58]. Typical narrow-ridge or broad area T1 lasers from SUNY with 3 active QWs emitting at $\lambda = 3.15$-3.4 μm [38], [39] operated at threshold voltage 0.8-1.4 V, whereas U. Montpellier reported a slightly higher V_{th} of 1.6 V for a narrow-ridge device with 2 QWs and emitting at 3.04 μm [59]. From these data we can estimate approximate excess voltage ratios for different wavelength ranges: $\gamma_V \equiv eV_{th}/\hbar\omega \approx 1.5$ (where $\hbar\omega$ is the photon energy) for devices emitting at 2.0-2.5 μm, ≈ 1.8 for devices spanning 2.5-3.0 μm, and > 2.0 (up to 4.0) for the less mature T1 devices operating at 3.0-3.5 μm. By contrast, threshold voltages for the broad area T2 ICLs emitting at $\lambda = 3.2$-4.0 μm from [18] typically fall in the range 2.1-2.4 V for 5-stage ICLs and 3.4-3.9 V for 7-stage ICLs. These values imply $\gamma_V \approx 1.4M$, where M is the number of stages. More specifically, $\gamma_V \approx 6.8$ for 5-stage ICLs and ≈ 9.8 for 7-stage devices. Since 5-stage ICLs perform quite well when low drive power is a key figure of merit, we can roughly convert the relative j_{th} for T2 *vs.* T1 QWs to relative P_{th} by multiplying the T2QW current densities by ≈ 4.4 in the range $\lambda = 2.0$-2.5 μm, by ≈ 3.8 in the range 2.5-3.0 μm, and by ≤ 3.3 in the range 3.0-3.5 μm. Following application of these factors to the j_{th} data shown in Fig. 3, we conclude that P_{th} for state-of-the-art T1 and T2 QW lasers are roughly equal at $\lambda \approx 3.3$ μm.

Furthermore, threshold power density represents only one figure of merit for mid-IR laser performance. Other key attributes are governed by the performance above threshold, such as maximum cw power attainable with good beam quality and maximum wallplug efficiency (WPE). While direct comparisons between lasers of different types that are designed and fabricated at different facilities are never possible due to inevitable variations in the optical confinement factors, processing methods, cavity parameters, thermal management, *etc.*, a brief overview is nonetheless useful. At $\lambda \approx 2.0$ μm, T1QW diodes and T1 ICLs have produced cw output powers approaching 2 W and WPEs up to 20-30%, although most of those T1 reports studied broad area lasers (*e.g.*, 100 μm ridge width) that emitted in multiple lateral modes [30], [60], [61]. Broad-area T1QW diodes emitting at $\lambda \approx 2.4$ μm have emitted up to 1.05 W cw, with WPE up to 17.5% [35]. At $\lambda \approx 3.0$ μm, T1 ICLs generated maximum cw powers up to 960 mW (WPE $\approx 11\%$), whereas at $\lambda \approx 3.3$ μm the maximum was 650 mW with WPE $\approx 16\%$ [60]. Narrow-ridge T1 ICLs emitted up to 107 mW (WPE $\approx 9.7\%$) at $\lambda \approx 2.97$ μm [62] and 85 mW at $\lambda \approx 3.25$ μm [60]. By comparison, narrow-ridge T2 ICLs that emitted in a high-quality beam have demonstrated cw power > 500 mW and WPE up to 18% [63]. WPEs exceeding 10% have been routine for narrow-ridge T2 ICLs with wavelengths as short as 3.1 μm and as long as 3.7 μm. The internal loss of 3-5 cm^{-1} for T2 ICLs emitting between 3.1 and 3.7 μm [18] is somewhat lower than the values reported for T1QW lasers operating beyond 3 μm [60], [62].

We finally note that if the energy gap of the T1 well material can be reduced, *e.g.*, by substituting a dilute nitride, dilute bismide, or metamorphic InAsSb grown on a buffer with lattice constant between those of GaSb and InSb, the QW thickness could be decreased for greater subband separation and lower fraction of the carriers populating non-lasing subbands. On the other hand, we see from Fig. 6 that T2 ICLs of the current generation become disadvantageous at wavelengths $\lambda \leq 3.0$ μm due to the unexplained increase of j_{th} in that range. However, once the source of that unexpected increase is identified, it may become possible to redesign the structures for more competitive performance at shorter wavelengths.

VII. Conclusion

We have clarified and quantified the physical mechanisms determining threshold current and power densities in narrow-gap type-I and type-II QW lasers, which are emerging as central components in a new generation of compact mid-IR optoelectronic systems. While most of the dominant concepts and mechanisms have been discussed previously with regard to

one laser type or the other, this work's focus on the differences provides a more realistic assessment of fundamental factors limiting the present designs.

We have compared the Auger coefficients derived by analyzing T1 and T2 QW laser thresholds to other mid-IR values from the literature. Assuming non-degenerate statistics and equal electron and hole populations, the Auger decay rate in a QW is $\tau_A^{-1} \approx C_{2D} n^2$. This expression is generally accurate for photodetectors with absorber carrier densities far below the degenerate limit. It is less accurate in lasers that operate near the onset of degeneracy and, for this reason, can produce a slight underestimate of the "true" low-density Auger coefficient. This is particularly true for lasers with low confinement factors (few wells or stages) and higher cavity loss. Considering the difficulty of establishing the full carrier-density dependence of the Auger rate in these structures, we believe that our approach is a reasonable approximation.

It is often useful to convert the 2D Auger coefficient derived in this manner to a 3D value so a tentative comparison can be made to Auger coefficients in other systems including superlattices and bulk materials. This is accomplished by defining a "normalization length" that accounts for the spatial extent of the electron and hole wavefunctions. The comparison of 3D Auger coefficients in Fig. 4 confirms that the non-radiative decay is substantially suppressed in both QW types, which occurs because compressive strain lifts the degeneracy of the heavy and light hole subbands as shown in Figs. 1 and 2. The much lighter in-plane effective mass for holes near the top of the valence band introduces a substantial activation energy for Auger recombination at room temperature.

The plot in Fig. 5 of 2D Auger coefficients for both QW types indicates lower T1QW values to wavelengths beyond 3.5 μm. However, this does not necessarily imply a lower lasing threshold because T1QW lasers must inject more carriers to produce enough gain for lasing. Only a fraction of the injected carriers (especially holes) occupy the extremal conduction and valence subbands, whereas nearly all of the electrons and holes injected into a T2QW laser occupy the most favorable subbands. The plot of T1 and T2 QW lasing thresholds in Fig. 6 indicates that when all of these considerations are combined, the thresholds governed by Auger recombination cross over near $\lambda \approx 3.1$ μm. But even this finding must be taken with a grain of salt, because T2 ICLs generally require higher operating voltage than T1 diodes. Hence their threshold power density may be higher even when the threshold current density is lower. Nonetheless, T1 ICLs, which also require higher operating voltages, have often provided the best performance results ($e.g.$, WPE) for T1QW lasers emitting beyond 3.0 μm.

Other factors such as maximum output power, wallplug efficiency, and manufacturability related to the growth and processing of single-mode or high-power devices must also naturally be considered in choosing which QW type should be employed for a given application at a given wavelength. Since the lasers of both types are still far from fully mature, ongoing performance improvements may further shift the balance. At $\lambda > 3.0$ μm, the T1QW lasers are limited by a substantial injection of carriers into non-lasing subbands, whereas at $\lambda < 3.2$ μm the T2QW devices are limited by some unknown mechanism that causes both the Auger coefficient and internal loss to increase with decreasing wavelength.

ACKNOWLEDGMENT

The authors would like to thank Kenneth Underwood and Juliet Gopinath for providing the data from [17] in digital form.

REFERENCES

[1] I. Vurgaftman *et al.*, "Sensitive chemical detection with distributed feedback interband cascade lasers," in *Encyclopedia of Analytical Chemistry: Applications, Theory and Instrumentation*, R. A. Meyers, Ed. Chichester, U.K.: Wiley, 2016, doi: 10.1002/9780470027318.a9559).

[2] M. von Edlinger *et al.*, "Interband cascade lasers for applications in process control and environmental monitoring," in *Proc. Energy Environ. Congr.*, 2015, p. EM2A-5, doi: 10.1364/EE.2015.EM2A.5.

[3] B. Henderson *et al.*, "Laser spectroscopy for breath analysis: Towards clinical implementation," *Appl. Phys. B, Lasers Opt.*, vol. 124, no. 8, pp. 161, Aug. 2018.

[4] J. Wagner *et al.*, "Infrared semiconductor lasers for DIRCM applications," *Proc. SPIE*, vol. 7115, Oct. 2008, Art. no. 71150A.

[5] P. Martyniuk, J. Antoszewski, M. Martyniuk, L. Faraone, and A. Rogalski, "New concepts in infrared photodetector designs," *Appl. Phys. Rev.*, vol. 1, no. 4, Dec. 2014, Art. no. 041102.

[6] N. Orazi, "Mid-wave infrared reflectography and thermography for the study of ancient books: A review," *Stud. Conservation*, vol. 65, no. 8, pp. 437–449, Nov. 2020.

[7] L. Pincherle, "Auger effect in semiconductors," *Proc. Phys. Soc., Sect. B*, vol. 68, no. 5, pp. 319–320, May 1955.

[8] I. Vurgaftman, M. P. Lumb, and J. R. Meyer, *Bands and Photons in III-V Semiconductor Quantum Structures*. London, U.K.: Oxford Univ. Press, 2021.

[9] Y.-G. Zhou, X.-Y. Zhao, C.-F. Cao, Q. Gong, and C. Wang, "High optical feedback tolerance of InAs/GaAs quantum dot lasers on germanium," *Opt. Exp.*, vol. 26, no. 21, p. 28131, Oct. 2018.

[10] T. N. Casselman, "Calculation of the auger lifetime in p-type $Hg_{1-x}Cd_xTe$," *J. Appl. Phys.*, vol. 52, no. 2, pp. 848–854, Feb. 1981.

[11] C. H. Grein, P. M. Young, and H. Ehrenreich, "Minority carrier lifetimes in ideal InGaSb/InAs superlattices," *Appl. Phys. Lett.*, vol. 61, no. 24, pp. 2905–2907, Dec. 1992.

[12] E. R. Youngdale *et al.*, "Auger lifetime enhancement in InAs-$Ga_{1-x}In_xSb$ superlattices," *Appl. Phys. Lett.*, vol. 64, no. 23, p. 3160, 1994.

[13] M. E. Flatté, C. H. Grein, H. Ehrenreich, R. H. Miles, and H. Cruz, "Theoretical performance limits of 2.1–4.1 μm InAs/InGaSb, HgCdTe, and InGaAsSb lasers," *J. Appl. Phys.*, vol. 78, no. 7, pp. 4552–4559, Oct. 1995.

[14] R. G. Bedford, G. Triplett, D. H. Tomich, S. W. Koch, J. Moloney, and J. Hader, "Reduced auger recombination in mid-infrared semiconductor lasers," *J. Appl. Phys.*, vol. 110, no. 7, Oct. 2011, Art. no. 073108.

[15] I. Vurgaftman *et al.*, "Interband cascade lasers with low threshold powers and high output powers," *IEEE J. Sel. Topics Quantum Electron.*, vol. 19, no. 4, Jul. 2013, Art. no. 1200210.

[16] T. D. Eales *et al.*, "Wavelength dependence of efficiency limiting mechanisms in type-I mid-infrared GaInAsSb/GaSb lasers," *IEEE J. Sel. Topics Quantum Electron.*, vol. 23, no. 6, Nov. 2017, Art. no. 1500909.

[17] K. J. Underwood *et al.*, "Strain dependence of auger recombination in 3 μm GaInAsSb/GaSb type-I active regions," *Appl. Phys. Lett.*, vol. 116, no. 26, Jun. 2020, Art. no. 262103.

[18] J. R. Meyer *et al.*, "The interband cascade laser," *Photonics*, vol. 7, no. 3, p. 75, 2020.

[19] T. D. Eales, I. P. Marko, A. R. Adams, J. R. Meyer, I. Vurgaftman, and S. J. Sweeney, "Auger recombination coefficients in type-I mid-infrared InGaAsSb quantum well lasers," *J. Phys. D*, vol. 54, no. 5, 2021, Art. no. 055105.

[20] I. Vurgaftman, J. R. Meyer, and L.-R. Ram-Mohan, "Band parameters for III-V compound semiconductors and their alloys," *J. Appl. Phys.*, vol. 89, no. 11, p. 5815, 2001.

[21] J. R. Meyer, C. A. Hoffman, F. J. Bartoli, and L. R. Ram-Mohan, "Type-II quantum-well lasers for the mid-wavelength infrared," *Appl. Phys. Lett.*, vol. 67, no. 6, p. 757, 1995.

[22] J. R. Meyer *et al.*, "Auger coefficients in type-II InAs/$Ga_{1-x}In_xSb$ quantum wells," *Appl. Phys. Lett.*, vol. 73, no. 20, pp. 2857–2859, Nov. 1998.

[23] W. W. Bewley *et al.*, "Lifetimes and Auger coefficients in type-II W interband cascade lasers," *Appl. Phys. Lett.*, vol. 93, no. 4, 2008, Art. no. 041118.

[24] M. E. Flatte *et al.*, "Carrier recombination rates in narrow-gap InAs/$Ga_{1-x}In_xSb$-based superlattices," *Phys. Rev. B, Condens. Matter*, vol. 59, no. 8, p. 5745, 1999.

[25] I. Vurgaftman *et al.*, "Rebalancing of internally generated carriers for mid-infrared interband cascade lasers with very low power consumption," *Nature Commun.*, vol. 2, no. 1, p. 585, Sep. 2011.

[26] R. Q. Yang, "Infrared laser based on intersubband transitions in quantum wells," *Superlattices Microstruct.*, vol. 17, no. 1, pp. 77–83, Jan. 1995.

[27] J. R. Meyer, I. Vurgaftman, R. Q. Yang, and L. R. Ram-Mohan, "Type-II and type-I interband cascade lasers," *Electron. Lett.*, vol. 32, no. 1, p. 45, 1996.

[28] J. R. Lindle, J. R. Meyer, C. A. Hoffman, F. J. Bartoli, G. W. Turner, and H. K. Choi, "Auger lifetime in InAs, InAsSb, and InAsSb-InAlAsSb quantum wells," *Appl. Phys. Lett.*, vol. 67, no. 21, pp. 3153–3155, Nov. 1995.

[29] G. L. Belenky, L. Shterengas, G. Kipshidze, and T. Hosoda, "Type-I diode lasers for spectral region above 3 μm," *IEEE J. Sel. Topics Quantum Electron.*, vol. 17, no. 15, pp. 1426–1434, Apr. 2011.

[30] L. Shterengas *et al.*, "Cascade pumping of 1.9-3.3 μm type-I quantum well GaSb-Based diode lasers," *IEEE J. Sel. Topics Quantum Electron.*, vol. 23, no. 3, Mar. 2017, Art. no. 1500708.

[31] E. Tournié and A. N. Baranov, *Advanced Semiconductor Lasers*, J. J. Coleman, C. A. Bryce, and C. Jagadish, Eds. Amsterdam, The Netherlands: Elsevier, 2012, pp. 183–226.

[32] C. L. Canedy *et al.*, "Interband cascade lasers with longer wavelengths," *Proc. SPIE*, vol. 10111, Jan. 2017, Art. no. 10111G.

[33] G. W. Turner, H. K. Choi, and M. J. Manfra, "Ultralow-threshold strained singlequantum-well GaInAsSb/AlGaAsSb lasers emitting at 2.05 μm," *Appl. Phys. Lett.*, vol. 72, no. 8, p. 876 1998.

[34] K. O'Brien *et al.*, "Recombination processes in midinfrared InGaAsSb diode lasers emitting at 2.37 μm," *Appl. Phys. Lett.*, vol. 89, no. 5, Jul. 2006, Art. no. 051104.

[35] L. Shterengas, G. Belenky, M. V. Kisin, and D. Donetsky, "High power 2.4 μm heavily strained type-I quantum well GaSb-based diode lasers with more than 1W of continuous wave output power and a maximum power-conversion efficiency of 17.5%," *Appl. Phys. Lett.*, vol. 90, no. 1, Jan. 2007, Art. no. 011119.

[36] L. Shterengas, G. Belenky, G. Kipshidze, and T. Hosoda, "Room temperature operated 3.1 μm type-I GaSb-based diode lasers with 80 mW continuous-wave output power," *Appl. Phys. Lett.*, vol. 92, no. 17, Art. no. 171111, 2008.

[37] T. Hosoda, G. Belenky, L. Shterengas, G. Kipshidze, and M. V. Kisin, "Continuous-wave room temperature operated 3.0 μm type I GaSb-based lasers with quinternary AlInGaAsSb barriers," *Appl. Phys. Lett.*, vol. 92, no. 9, Mar. 2008, Art. no. 091106.

[38] J. Chen *et al.*, "2.7-μm GaSb-based diode lasers with quinary waveguide," *IEEE Photon. Technol. Lett.*, vol. 21, no. 16, pp. 1112–1114, Jul. 2009.

[39] R. Liang, T. Hosoda, G. Kipshidze, L. Shterengas, and G. Belenky, "GaSb-based diode lasers with asymmetric separate confinement heterostructure," *IEEE Photon. Technol. Lett.*, vol. 25, no. 10, pp. 925–928, Apr. 2013.

[40] I. Šimonytė *et al.*, "Single-frequency infrared tunable lasers with single-angle-facet gain chips for sensing applications," *Proc. SPIE*, vol. 10111, Jan. 2017, Art. no. 101110H.

[41] S. Hausser, G. Fuchs, A. Hangleiter, K. Streubel, and W. T. Tsang, "Auger recombination in bulk and quantum well InGaAs," *Appl. Phys. Lett.*, vol. 56, no. 10, pp. 913–915, Mar. 1990.

[42] Y. Zou *et al.*, "Effect of Auger recombination and differential gain on the temperature sensitivity of 1.5 μm quantum well lasers," *Appl. Phys. Lett.*, vol. 62, no. 2, p. 175, 1993.

[43] J. Piprek, *Semiconductor Optoelectronic Devices*. New York, NY, USA: Springer, 2003, ch. 3.

[44] K. L. Vodopyanov, H. Graener, C. C. Phillips, and T. J. Tate, "Picosecond carrier dynamics and studies of auger recombination processes in indium arsenide at room temperature," *Phys. Rev. B*, vol. 46, no. 20, pp. 13194–13200, Nov. 1992.

[45] E. E. Vdovkina, N. S. Baryshev, M. P. Shchetinin, A. P. Cherkasov, and I. S. Aver'yanov, "Photoelectric properties of $CdxHg_{1-x}Te$ at high temperatures," *Sov. Phys. Semicond.*, vol. 10, no. 1, p. 109, 1976.

[46] J. Bajaj, S. H. Shin, J. G. Pasko, and M. Khoshnevisan, "Minority carrier lifetime in LPE $H_{1-x}Cd_xTe$," *J. Vac. Sci. Technol. A, Vac., Surf., Films*, vol. 1, no. 3, p. 1749, 1983.

[47] M. E. de Souza, M. Boukerche, and J. P. Faurie, "Minority carrier lifetime in *p*-type (111) HgCdTe grown by molecular beam epitaxy," *J. Appl. Phys.*, vol. 68, no. 10, p. 5195, 1990.

[48] J. Bonnet-Gamard, J. Bleuse, N. Magnea, and J. L. Pautrat, "Optical gain and laser emission in HgCdTe heterostructures," *J. Appl. Phys.*, vol. 78, no. 12, pp. 6908–6915, Dec. 1995.

[49] J. L. Pautrat, E. Hadji, J. Bleuse, and N. Magnea, "Resonant-cavity infrared optoelectronic devices," *J. Electron. Mater.*, vol. 26, no. 6, pp. 667–672, Jun. 1997.

[50] R. Klann, T. Höfer, R. Buhleier, T. Elsaesser, and J. W. Tomm, "Fast recombination processes in lead chalcogenide semiconductors studied via transient optical nonlinearities," *J. Appl. Phys.*, vol. 77, no. 1, pp. 277–286, Jan. 1995.

[51] P. C. Findlay *et al.*, "Auger recombination dynamics of lead salts under picosecond free-electron-laser excitation," *Phys. Rev. B, Condens. Matter*, vol. 58, no. 19, pp. 12908–12915, Nov. 1998.

[52] S. J. Sweeney *et al.*, "Dependence of threshold current on QW position and on pressure in 1.5 μM InGaAs(P) lasers," *Phys. Status Solidi b*, vol. 211, no. 1, pp. 525–531, Jan. 1999.

[53] I. Vurgaftman *et al.*, "Interband cascade lasers," *J. Phys. D, Appl. Phys.*, vol. 48, no. 12, 2015, Art. no. 123001.

[54] Z. L. Bushell, "Development of novel infrared photonic materials and devices," M.S. thesis, Dept. Phys., Univ. Surrey, Guildford, U.K., 2017.

[55] Z. L. Bushell *et al.*, "Pressure-dependent properties of type-II InAs/GaInSb mid-infrared interband cascade light-emitting devices," *Proc. SPIE*, vol. 10111, Apr. 2017, Art. no. 101110L.

[56] S. Jung, G. Kipshidze, R. Liang, S. Suchalkin, L. Shterengas, and G. Belenky, "GaSb-based mid-infrared single lateral mode lasers fabricated by selective wet etching technique with an etch stop layer," *J. Electron. Mater.*, vol. 41, no. 5, pp. 899–904, May 2012.

[57] R. M. Briggs *et al.*, "Single-mode 2.65 μm InGaAsSb/AlInGaAsSb laterally coupled distributed-feedback diode lasers for atmospheric gas detection," *Opt. Exp.*, vol. 21, no. 1, p. 1317, 2013.

[58] K. Vizbaras *et al.*, "MBE growth of low threshold GaSb-based lasers with emission wavelengths in the range of 2.5–2.7 μm," *J. Cryst. Growth*, vol. 323, no. 1, pp. 446–449, May 2011.

[59] Q. Gaimard *et al.*, "Distributed feedback GaSb based laser diodes with buried grating: A new field of single-frequency sources from 2 to 3 μm for gas sensing applications," *Opt. Exp.*, vol. 23, no. 15, p. 19118, Jul. 2015.

[60] L. Shterengas, T. Hosoda, M. Wang, T. Feng, G. Kipshidze, and G. Belenky, "High-power 1.9–3.3 μm type-I quantum-well cascade diode lasers," *Proc. SPIE*, vol. 10123, Feb. 2017, Art. no. 101230P.

[61] M. T. Kelemen *et al.*, "Diode laser arrays for 1.8 to 2.3 μm wavelength range," *Proc. SPIE*, vol. 7483, Sep. 2009, Art. no. 74830C.

[62] R. Liang *et al.*, "Narrow ridge $\lambda \approx$ 3-μm cascade diode lasers with output power above 100 mW at room temperature," *IEEE Photon. Technol. Lett.*, vol. 27, no. 23, pp. 2425–2428, Aug. 2015.

[63] M. Kim *et al.*, "High-power continuous-wave interband cascade lasers with 10 active stages," *Opt. Exp.*, vol. 23, no. 8, p. 9664, Apr. 2015.

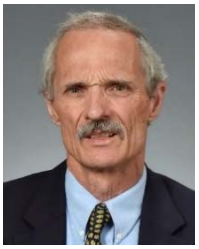

Jerry R. Meyer (Fellow, IEEE) received the Ph.D. degree in physics from Brown University in 1977. Since 1977, he has carried out basic and applied research at the Naval Research Laboratory, Washington, DC, USA, where he is currently the Navy Senior Scientist of quantum electronics (ST). His investigations have focused on semiconductor optoelectronic materials and devices, such as developing new classes of semiconductor lasers and detectors for the infrared. He has coauthored more than 380 refereed journal articles which have been cited more than 27 000 times (H-index of 65), 39 patents, and more than 190 invited conference presentations. He has coauthored the book *Bands and Photons in III-V Semiconductor Quantum Structures* (Oxford University Press, 2021). He is a fellow of the Optical Society of America, the American Physical Society, and the Institute of Physics.

Chadwick L. Canedy received the B.A. degree in physics and mathematics from Wesleyan University, Middletown, CT, USA, in 1992, and the Ph.D. degree in physics from Brown University, Providence, RI, USA, in 1998. He was a Post-Doctoral Fellow with the University of Maryland, investigating complex oxides for microwave communication applications and their integration with silicon technologies. He has been a Research Physicist with the Optical Sciences Division, U.S. Naval Research Laboratory, Washington, DC, USA, since 2001, where he has focused on the molecular beam epitaxy of III-V materials for optoelectronics, in particular, new types of emitters and detectors operating in the infrared. He has coauthored 110 refereed journal articles, four book chapters, 19 patents, and more than 90 invited conference presentations. His work has more than 5000 citations (H-index of 41). His dissertation research centered on the study of the magneto-transport properties in artificially structured materials, such as sputtered magnetic superlattices and laser ablated complex oxides. He is a member of the American Physical Society.

Mijin Kim received the Ph.D. degree in physics from the University of Notre Dame, Notre Dame, IN, USA, in 2002. She has been working with the U.S. Naval Research Laboratory, Dr. Meyer's Group, Washington, DC, USA, since she was awarded the National Research Council Postdoctoral Fellowship, in 2002. In 2006, she joined as a Physicist with the U.S. Naval Research Laboratory. Her current research interests include optoelectronic devices, such as semiconductor photonic crystals, plasmonics, and mid-IR cascade lasers.

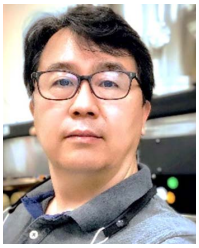

Chul Soo Kim received the Ph.D. degree in physics from the University of Notre Dame, Notre Dame, IN, USA, in 2000. His Ph.D. research focused on II-VI semiconductor low dimensional quantum structures grown by molecular beam epitaxy (MBE). From 2000 to 2002, he was a National Research Council Post-Doctoral Fellow with the National Institute of Standards and Technology, Boulder, CO, USA. He is currently a Research Physicist with the Quantum Optoelectronics Section, Naval Research Laboratory (NRL), Washington, DC, USA. His bibliography includes 150 refereed publications, 11 patents and two patent applications, four book chapters, 55 invited, and 102 contributed conference presentations. His publications have been cited more than 4942 times yielding an H-index of 38. His research interests include interband and quantum cascade lasers, optoelectronics, nano-photonics, and plasmonic devices. He is a member of the American Physical Society and the Optical Society.

Charles D. Merritt was born in San Bernardino, CA, USA. He received the B.S. degree in chemistry from the University of California at Riverside, Riverside, CA, USA, and the Ph.D. degree in chemistry from The Catholic University of America. He has been with the Naval Research Laboratory since 1987. During that time he has worked in the areas of energetic materials reaction mechanisms, optical phenomena of aerosol droplets, matrix isolation spectroscopy of reactive intermediates, organic light emitting diode characterization, photonic crystal fiber fabrication and testing, aerosol particle capture technology, and mid-IR semiconductor lasers characterization. His 58 refereed journal articles have a citation H-index of 25.

William W. Bewley received the Ph.D. degree from the University of California at Santa Barbara, Santa Barbara, CA, USA, in 1993. Since 1997, he has been with the Naval Research Laboratory, Washington, DC, USA, where he leads the characterization of semiconductor lasers and detectors, infrared frequency combs, super-radiant quantum wells, and negative-photoluminescence devices. His 126 refereed journal articles have a citation H-index of 33.

Igor Vurgaftman is currently the Head of the Optical Sciences Division, Quantum Optoelectronics Section, NRL, where he investigates type-II superlattice photodetectors, mid-IR lasers based on inter-band and inter-sub-band transitions, and the fundamental physics of a wide variety of plasmonic and polaritonic devices. He has coauthored the book *Bands and Photons in III-V Semiconductor Quantum Structures* (Oxford University Press, 2021), more than 285 refereed articles in technical journals, which have been cited more than 13 000 times (H-index of 46), as well as 23 patents granted. He is a fellow of the Optical Society of America and the American Physical Society. He was a recipient of the Dr. Dolores M. Etter Top Navy Scientists and Engineers of the Year Award in 2015, the NRL Sigma Xi Pure Science Award in 2012, the IEEE Photonics Society Engineering Achievement Award in 2012, and the NRL Sigma Xi Young Investigator Science Award in 2005.